POLITECNICO DI TORINO
Repository ISTITUZIONALE

Performance analysis of the NbTi PF coils for the EU DEMO fusion reactor

Original
Performance analysis of the NbTi PF coils for the EU DEMO fusion reactor / Zappatore, A., Bonifetto, R., Bruzzone, P., Corato, V., Di Zenobio, A., Savoldi, L., Sedlak, K., Turtu, S., Zanino, R.. - In: IEEE TRANSACTIONS ON APPLIED SUPERCONDUCTIVITY. - ISSN 1051-8223. - STAMPA. - 28:4(2018), p. 4901005. [10.1109/TASC.2018.2793462]

Availability:
This version is available at: 11583/2697869 since: 2018-02-26T10:21:19Z

Publisher:
Institute of Electrical and Electronics Engineers Inc.

Published
DOI:10.1109/TASC.2018.2793462

Terms of use:

This article is made available under terms and conditions as specified in the corresponding bibliographic description in the repository

Publisher copyright
IEEE postprint/Author's Accepted Manuscript

©2018 IEEE. Personal use of this material is permitted. Permission from IEEE must be obtained for all other uses, in any current or future media, including reprinting/republishing this material for advertising or promotional purposes, creating new collecting works, for resale or lists, or reuse of any copyrighted component of this work in other works.

(Article begins on next page)

13 October 2026

Performance analysis of the NbTi PF coils for the EU DEMO fusion reactor

A. Zappatore, R. Bonifetto, P. Bruzzone, V. Corato, A. Di Zenobio, L. Savoldi, *Member, IEEE,* K. Sedlak, S. Turtù, *Senior Member, IEEE* and R. Zanino, *Senior Member, IEEE*

***Abstract*— The first design of the NbTi Poloidal Field (PF) coils for the EU DEMO fusion reactor has been proposed by the Swiss Plasma Center (SPC) and by the Italian National Agency for New Technologies, Energy and Sustainable Economic Development (ENEA). The thermal-hydraulic (TH) performance analysis of the PF coil system presented in this work has been carried out using the state-of-the-art 4C code. The minimum temperature margin and the TH response of the coils to the heat deposition due to AC losses are computed in two different plasma scenarios, using a single time constant ($n\tau$) whose value is currently unknown. Therefore, we apply our model to parametrically assess the sensitivity of the PF performance to a range of $n\tau$ values. The calculations are also performed taking into account that the high void fraction design of the conductor leads to the opening of a channel due to the Lorentz force. For all situations considered here, the 4C code predicts that the temperature margin never goes below the acceptable minimum of 1.5 K**

***Index Terms*— Nuclear fusion reactor, EU DEMO, Superconducting magnets, Thermal-hydraulic analysis, 4C code.**

I. Introduction

THE pre-conceptual design of the six superconducting (SC) Poloidal Field (PF) coils of the EU DEMO fusion reactor is being developed by the SPC (Swiss Plasma Center) and ENEA (Italian National Agency for New Technologies, Energy and Sustainable Economic Development), in the framework of the EUROfusion work package magnets (WPMAG).

The preliminary design of the winding pack (WP) of each PF coil consists of a stack of NbTi cable-in-conduit conductors (CICCs). The pulsed operation of the PF and CS coils induces AC losses in the conductors. The coupling losses can be estimated by means of their coupling time constant $n\tau$. The latter is at present unknown to the proposed conductor design, but it is of paramount importance in the determination of the heat load and consequently of the cable operating temperature.

In this work, the thermal-hydraulic (TH) model of the PF coils is developed using the 4C code [1], based on the current status of the PF system design.

The nominal operation of the coils is simulated during a series of plasma pulses until periodicity is reached in two different scenarios for the given evolution of the operating current and accounting for the AC losses induced by the magnetic field variation.

Two sensitivity studies are finally presented: one varying parametrically the conductor $n\tau$, aimed at assessing, for the given WP configuration, the maximum affordable $n\tau$ value that allows to satisfy the minimum temperature margin constraint of 1.5 K during pulsed operation; the other aimed at assessing the impact of the channel opening due to Lorentz force, on both the temperature margin and the mass flow rate distribution among the different PF coils.

II. The ENEA-SPC design of the EU DEMO PF coils

The PF coil system is composed by six coils, numbered from 1 to 6 (top to bottom), see Fig. 1. Each PF coil is layer-wound following a multiple-in-hand winding technique, in order to keep the hydraulic length sufficiently low (< 500 m), see Table I and Fig. 2(a). This approach has already been followed in the ITER PF design [2].

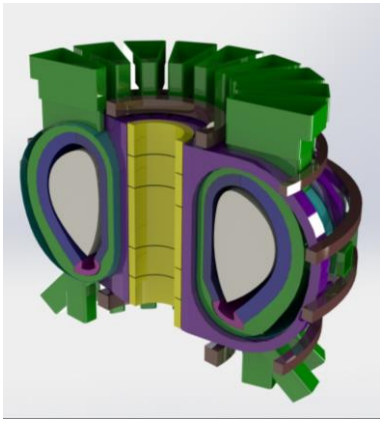

Fig. 1. CAD model of the EU DEMO fusion reactor. The six PF coils are colored in brown.

This work has received funding from the Euratom research and training programme 2014-2018 under grant agreement No 633053. This work has been carried out within the framework of the EUROfusion Consortium. The views and opinions expressed herein do not necessarily reflect those of the European Commission. *(Corresponding author: R. Zanino.)*

A. Zappatore, R. Bonifetto, L. Savoldi and R. Zanino are with the NEMO Group, Dipartimento Energia, Politecnico di Torino, 10129 Torino, Italy (e-mail roberto.zanino@polito.it).

P. Bruzzone and K. Sedlak are with SPC EPFL, Villigen 5232, Switzerland.

V. Corato, A. Di Zenobio and S. Turtù are with ENEA, 00044 Frascati, Italy,

Color versions of one or more of the figures in this paper are available online at http://ieeexplore.ieee.org .

Digital Object Identifier will be inserted here upon acceptance.

Template version 8.0, 27 July 2017. IEEE will put copyright information in this area
See http://www.ieee.org/publications_standards/publications/rights/indes.html for more information.

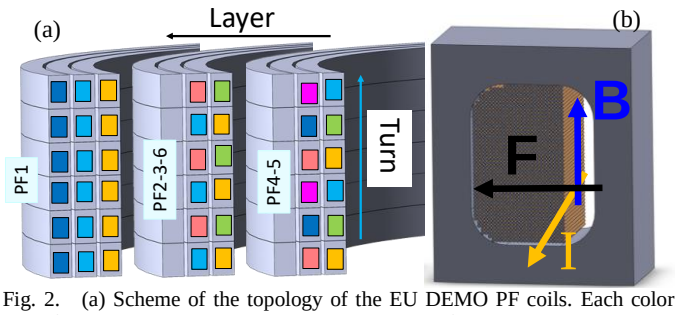

Fig. 2. (a) Scheme of the topology of the EU DEMO PF coils. Each color identifies one hydraulic channel. (b) Cross section of a PF1 conductor with the open channel due to Lorentz force (F) caused by the magnetic field (B) and current (I).

The PF conductors are forced-flow He-cooled NbTi cable-in-conduit conductors (CICCs), without a low impedance channel but with a high void fraction (40%), see Table II. The Lorentz force should then compact the strands (1 mm diameter) towards the outer side of the jacket and therefore opening of a low-impedance channel on the inner side of the CICC, see Fig. 2(b), as already assumed to explain some experimental observations in the first ITER CS Insert Coil [3]. It is worth noting that we are considering the extreme case in which the (untwisted) NbTi moves rigidly. In a more detailed model, the real twist pitch as well as the stiffness, higher than Nb_3Sn strands, should be taken into account.

III. 4C Model and Simulation Setup

A. Coil

In each PF coil, all conductors are supposed to be cooled in parallel.

The thermal coupling between neighboring turns and layers is taken into account through a series of thermal resistances, given by the turn and layer insulation.

The constitutive law for the friction factor inside the cable bundle, based on the porous media analogy, is taken from [4].

The parameterization of the critical surface of the NbTi is taken from [5] assuming the following coefficients: $C_0 = 1.685 \cdot 10^{12}$ A·T/m^2, $B_{c20} = 14.61$ T, $T_{c0} = 9.03$ K, $\alpha = 1.0$, $\beta = 1.54$, $\gamma = 2.1$, $n = 1.7$, which are the same of the NbTi ITER conductors, being the EU DEMO PF design at its pre-conceptual stage.

For this preliminary assessment, the Cu/NonCu ratio in the SC strands has been assumed equal to 1, as well as the $\cos(\theta)$, where θ is the average twist pitch angle.

In the first part of the analysis, the effect of the channel opening due to current and magnetic field inside the conductor is neglected, then a first assessment of this effect is performed. We assume that the motion of the strands bundle, i.e. the dimension of the opening channel, is directly proportional to the Lorentz force. Note that this is a simplifying assumption and a dedicated model/experiment would be necessary. We assume, also, that the maximum compaction of the strands leads to a void fraction of $1 - \pi/4 \sim 21\%$, corresponding to a square lattice with all the (rigid) strands in contact to their four 4 neighbors.

The friction factor adopted for the resulting low-impedance channel, of assumed rectangular shape, is computed from the Petukhov correlation [6].

TABLE I
Main Coil Parameters

Coil	Coil radius (m)	Number of layers/turns	Hydraulic length (m)	#-in-hand	Maximum current (kA)
PF1	5.4	16/14	475	1	55.3
PF2	14	14/10	440	2	57.1
PF3	17	8/8	427	2	53.3
PF4	17	14/12	427	3	54.9
PF5	14.4	12/12	362	3	53.8
PF6	7.0	20/16	352	2	

TABLE II
Main Conductor Parameters

Coil	Helium cross section (mm^2)	Number of SC strands	Number of Cu strands	Strand cross section (mm^2)	SC cross section (mm^2)
PF1	627.3	945	198	941.0	389.0
PF2	398.5	135	626	597.7	53.0
PF3	377.1	82	605	565.6	33.8
PF4	410.0	161	586	615.0	66.3
PF5	393.5	127	590	590.3	52.3
PF6	681.1	1027	214	1021.7	422.8

B. Cryogenic circuit

The 4C model of the cryogenic cooling circuit used to cool the PF coils, see Fig. 3, is built assembling components from the Cryogenics Modelica library available in 4C [7]. The six PF coils are cooled in parallel by the SHe forced by the cold circulator and re-cooled by an (ideal) heat exchanger. The circuit volumes (manifolds and cryolines) are obtained scaling those of the ITER PF-Correction Coil circuit (considering only the PF portion of the circuit) [8] with respect to the He volume contained inside the coils. The cold circulator operational point has been found imposing a pressure drop of 1 bar to each PF coil separately, in order to find the total mass flow rate (1.6 kg/s) in the feeding circuit of all the PF coils. Given the operational point of the circulator, an ITER-like parabolic characteristic has been adopted.

As initial conditions, a temperature of 4.5 K is prescribed, while the coil inlet and outlet pressure are set equal to 6 bar and 5 bar, respectively.

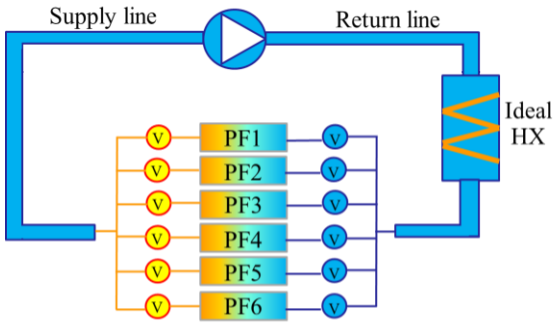

Fig. 3. Sketch of the 4C model of the EU DEMO PF coil system adopted in this work. The manifold volumes "V" at the coil inlets and outlets are also shown.

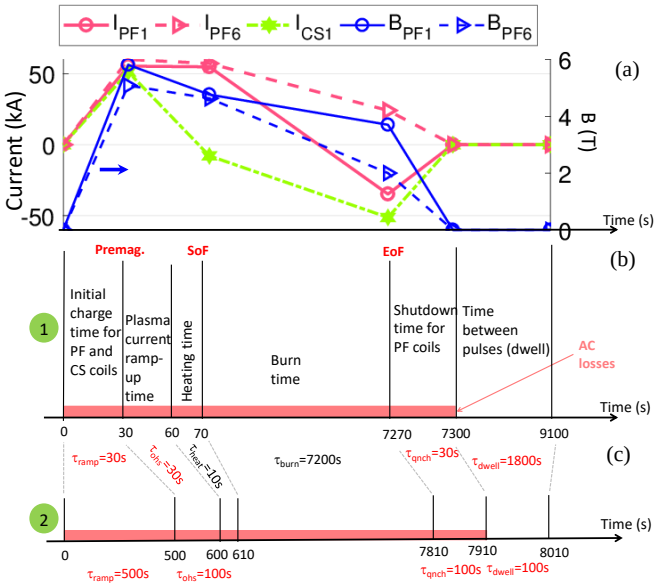

Fig. 4. (a) Current evolution in the first module of the CS (CS1) and the current and field evolution in PF1 and PF6 are also shown. (b, c) The two scenarios considered in this analysis. The characteristic times (τ_X) of each phase are called as in the PROCESS output. Phases with different duration in the two scenarios are highlighted in red.

C. Scenarios

The two plasma scenarios considered, see Fig. 4, are:

1. The outcome of a PROCESS simulation performed in 2015 [9], which is the baseline scenario adopted since then for the preconceptual design of the EU DEMO magnets
2. An updated scenario, that proposes a more realistic duration of the different phases [10], considering the power supply constraints.

The most relevant driver is the heat deposition due to the AC losses induced by the time-varying magnetic field, (see fig 4a, where the current and field variation are reported for PF1 and PF6 where we reach the highest losses). Note that all the relevant contributions to the magnetic field on the PF coils are accounted for here, and namely the self-field from pulsed operation of PF coils, the pulsed CS magnetic field, and, on top of that, the static contribution of the TF coils ripple.

In this analysis, the nuclear heat load coming from fusion reactions is neglected, being the PF coils far from the plasma, as well as hysteresis losses and eddy currents in the jacket and copper strands, since dedicated studies/experiment should be performed in the future to assess the sensitivity of the performance to these AC losses.

The AC losses contribution considered here are only the coupling losses, computed using the following relation [11]:

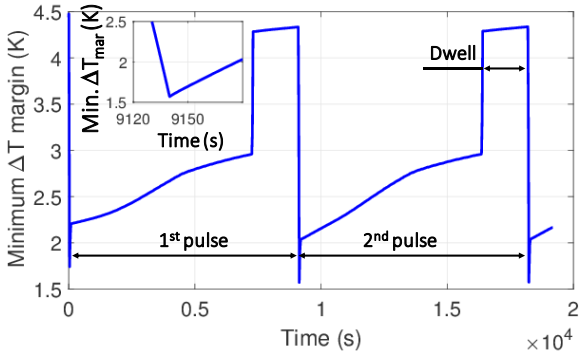

Fig. 5. Evolution of the minimum temperature margin during two plasma pulses of scenario 1 ($n\tau$ = 150 ms) in the first layer of the PF1. The inset shows on the premagnetization phase of the second plasma pulse.

$$Q'(x,t) = \frac{n\tau}{\mu_0}\left(\frac{\partial B(x,t)}{\partial t}\right)^2 A_{str} \quad \left[W/m\right] \tag{1}$$

where $n\tau$ (s) is the coupling time constant, μ_0 (H/m) is the vacuum permeability, B (T) is the magnetic field at point x and time t in each conductor and A_{str} (m^2) is the total cross section of the (superconducting + pure copper) strands.

The target minimum $n\tau$ value (before electromagnetic cycling) considered here is the ITER PF value (150 ms), but due to the lack of experimental data for the DEMO PF conductor several (larger) $n\tau$ values are also adopted parametrically, to give hints to the conductor designers about the maximum tolerable value.

The most critical phase from the point of view of the AC losses is the pre-magnetization. The reason is that the magnetic field in the conductor varies from 0 to its maximum value in a short time, 30 s in scenario 1, leading to large power deposition, see (1). On the other hand, the charge time of scenario 2 is much longer (500 s), therefore the power deposition is strongly reduced.

IV. Results

A. Temperature margin

The temperature margin ΔT_{mar} is computed as $\Delta T_{mar}(x,t) = T_{CS}(x,t) - T_{op}(x,t)$, where T_{CS} is the current sharing temperature and T_{op} is the strands operating temperature. The requirement to be satisfied is $min[\Delta T_{mar}(x,t)] \geq 1.5$ K, as already used in [12].

Starting from the initial condition, periodicity is reached already at the second plasma pulse, see Fig. 5. The reason is that the maximum transit time (PF1) is ~1 h which is half the burn time, during which almost no power is deposited. The transit time ranges from 4000 s to 2500 s moving from PF1 to PF6, respectively. The results discussed in this section are, therefore, extracted from the second pulse.

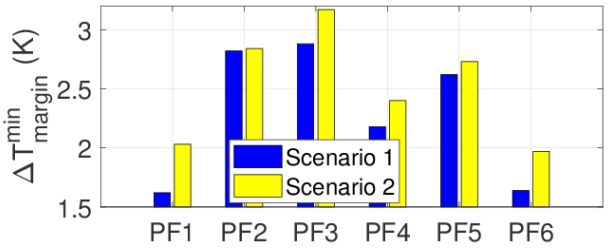

Fig. 6. Comparison of the minimum temperature margin in each PF coil between scenarios 1 and 2 ($n\tau$ = 150 ms). The minimum margin has to be considered as the absolute minimum in space and time in each coil.

The minimum ΔT_{mar} reached in each PF coil during the second pulse is reported in Fig. 6, showing that the ΔT_{mar} requirement is satisfied in all the coils. The location of the minimum margin is for all the coils in the first layer, because the maximum value of the magnetic field is reached there.

Comparing the two scenarios, the scenario 1, as discussed above, leads to higher power deposition, and therefore to higher temperatures. The ΔT_{mar} reduction is evident in PF1 and PF6, for which > 1 kW is deposited during the premagnetization phase in scenario 1, while < 0.1 kW is deposited in scenario 2, see Table III. On the other hand, the change in the ΔT_{mar} of PF2 and PF4 is less evident. This is due to the fact that the He volume present in those coils is high, therefore the temperature increase due to energy deposition of the helium is small. In addition, the energy deposited, see Table III, in PF2 and PF4 is rather small if compared to that of PF1 and PF6.

Note that the minimum ΔT_{mar} is located at the last turns of the conductors due to the magnetic field space distribution and the heating due to AC losses, see Fig 7.

B. *Hydraulics*

The PF coil system performance need to be assessed also from the hydraulic point of view. The steady state hydraulic performance of the coils is rather different, since 10 g/s and 14 g/s flow inside each channel of PF1 and PF6, respectively, while ~7 g/s are circulated in the channels of the remaining coils. The most loaded coils (PF1 and PF6) are those where more mass flow rate is circulated, but the remaining coils appear to be overcooled.

Only in the more critical scenario 1, backflow is predicted at the inlet of PF1 and PF6, see Fig. 8, due to the heat deposition in the premagnetization phase. Since the backflow involves only the first turns of PF1 and PF6, it does not affect the minimum temperature margin, which is located at the end of the hydraulic length (see again Fig. 7). However, the He expulsion could become an issue, if a secondary quench detection system should be adopted for the PF coil protection, based on the signal of the inlet flow meters as done in ITER [13].

C. *Parametric study on nτ*

The $n\tau$ values for the proposed PF conductors are obviously not known, as they exist at present only on paper. For this reason, a parametric study on the effects of increasing $n\tau$ has been performed in the case of the more severe scenario 1, see

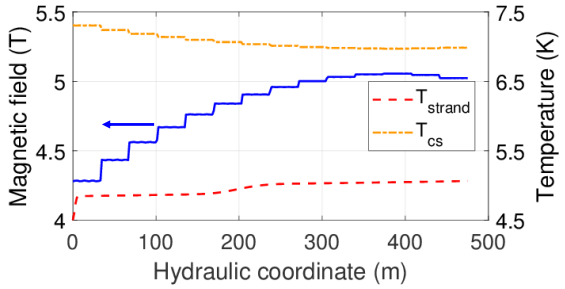

Fig. 7. Magnetic field distribution, strand temperature and current sharing temperature along the hydraulic length in the first layer of PF1 at the end of the premagnetization.

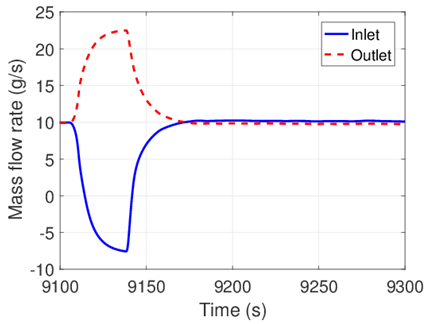

Fig. 8. Time evolution of the inlet and outlet mass flow rate in the first layer of the PF1coil during the pre-magnetization phase of the second pulse ($n\tau$ = 150 ms).

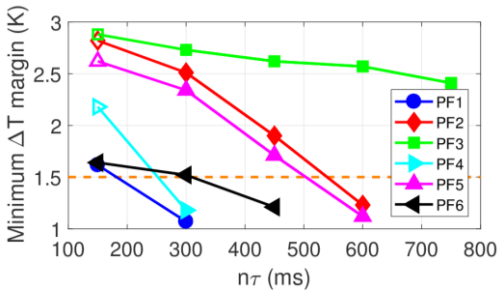

Fig. 9. Sensitivity of the PF coils performance to an increase of the coupling time constant $n\tau$ (scenario 1). Open symbols indicate no backflow at the coil inlet, solid symbols indicate the opposite.

Fig. 9, from which the maximum acceptable $n\tau$ and the possible condition of backflow at the coil inlet can be deduced for the current design.

D. *Effect of low-impedance channel opening*

As already described above, the presence of current and magnetic field leads to the opening of a low-impedance channel in the conduit.

TABLE III
POWER AND ENERGY DEPOSITED DURING A PLASMA PULSE

Coil	Max power deposited (W) in scenario 1/2	Total energy deposited (kJ) in scenario 1/2
PF1	1600/6	71/10
PF2	115/0.4	17/4.4
PF3	206/0.7	8.8/1.3
PF4	111/0.4	18/4.8
PF5	58/0.2	16/4.5
PF6	1512/5	50/4.1

The total mass flow rate during the plasma burn (when the channel is open) increases from 3% in PF6 to 18% in PF1. The mass flow rate in the (completely open) channel is for all the coils ~60% of the total, except for the PF3 in which it is ~40%, since the magnetic field and current in this coil are lower than the other, therefore the channel is smaller.

The effect on the margin of the channel opening is quite small, i.e. change in the $\Delta T_{mar} < 0.1$ K with respect to the case without channel opening. This can be explained by the fact that the channel is completely open during the plasma burn, but the power deposition in that frame is < 0.1 mW, so it is not relevant to have a higher mass flow rate. Similarly, when there is the highest power deposition, i.e. in PF1 and PF6 during premagnetization, the backflow is even worse, because the conductor hydraulic impedance is lower.

V. Conclusions

The 4C thermal-hydraulic model of the pre-conceptual design of the EU DEMO PF coils has been presented.

The predicted performance fulfills the minimum temperature margin requirement in both plasma scenarios considered in this paper, provided the coupling time constant $n\tau$ is not too large.

The heat loads considered in this analysis do not include all the possible contributions, i.e. eddy currents, nuclear heating or static loads, therefore further, more detailed investigations will be performed when these data will be available.

In one of the plasma scenarios considered, He backflow is predicted to arise at the inlet of some of the PF coils, as a consequence of the high heat deposition occurring because of AC losses in the pre-magnetization phase. This behavior should be taken into account in case of adoption of inlet backflow as secondary quench detection signal.

The possible opening of a low-impedance channel in the PF conductor, due to the Lorentz force acting on the cable, should not significantly affect the performance of the coils, according to the model.

References

[1] L. Savoldi Richard, F. Casella, B. Fiori, and R. Zanino, "The 4C code for the cryogenic circuit conductor and coil modeling in ITER," *Cryogenics*, vol. 50, no. 3, Mar. 2010, pp. 167-176.

[2] B. Lim, F. Simon, Y. Ilyin, C. Y. Gung, J. Smith, Y.H. Hsu, C. Luongo, C. Jong and N. Mitchell, "Design of the ITER PF coils," *IEEE Trans. Appl. Supercond.*, vol. 21, no. 3, Jun. 2011, pp. 1918-1921.

[3] K. Hamada, Y. Takahashi, K. Matsui, T. Kato, K. Okuno, "Effect of electromagnetic force on the pressure drop and coupling loss of a cable-in-conduit conductor," *Cryogenics*, vol. 44, no. 1, Jan. 2004, pp. 45-52.

[4] M. Lewandowska and M. Bagnasco, "Modified friction factor correlation for CICC's based on a porous media analogy," Cryogenics, vol. 51, no. 9, Sep. 2011, pp. 541-545.

[5] L. Bottura, "A Practical Fit for the Critical Surface of NbTi," *IEEE Trans. Appl. Supercond.*, vol. 10, no. 1, Mar. 2000, pp. 1054-1057.

[6] B. S. Petukhov, in T. F. Irvine and J.P. Hartnett, *Advances in Heat Transfer*. 7th ed., Wiley, Hoboken, NJ, 2009.

[7] R. Bonifetto, F. Casella, L. Savoldi, R. Zanino, "Dynamic modeling of a SHe closed loop with the 4C code," AIP Conference Proceedings, vol. 1434, 2012, pp. 1743-1750.

[8] F. Gauthier, D. Bessette, D.-K. Oh, "Thermal Hydraulic Analysis of the ITER PF and Correction Coils in 15 MA Scenario Operation Using the SuperMagnet Suite of Codes," *IEEE Trans. Appl. Supercond.*, vol. 24, no. 3, Jun. 2014, Art. no. 4201705.

[9] PROCESS system code run result, April 16th, 2015, DEMO1 Reference Design, Eurofusion IDM link: 2MDKFH.

[10] A. Ferro, "DEMO input power profiles", EUROfusion, Tech. Rep. EFDA_D_2MXL88, Dec. 15, 2017.

[11] A.M. Campbell, "A general treatment of losses in multifilamentary superconductors," *Cryogenics*, vol. 22, no. 1, Jan. 1982, pp. 3-16.

[12] L. Savoldi et al., "Perfomance analysis of a graded winding pack design for the EU DEMO TF coil in normal and off-normal conditions," *Fus. Eng. Des.*, vol. 124, pp. 45-48, 2017

[13] S. Nicollet et al. "Quench of ITER Poloidal Field coils: influence of some initiation parameters on thermo-hydraulic detection signals and main impact on cryogenic system", Cryogenics, vol. 53, 2013, pp. 86-93